Advances in Aircraft and Spacecraft Science, *Vol. 1, No. 1 (2014) 027-041*
DOI: http://dx.doi.org/10.12989/aas.2014.1.1.027

Circular cylinder drag reduction using piezoelectric actuators

Matteo Orazi[a], Davide Lasagna[b] and Gaetano Iuso[*]

Dipartimento di Ingegneria Meccanica e Aerospaziale, Politecnico di Torino
24, Corso Duca degli Abruzzi, 10129 Torino, Italy

(Received July 27, 2013, Revised September 25, 2013, Accepted October 3, 2013)

Abstract. An active flow control technique based on "smart-tabs" is proposed to delay flow separation on a circular cylinder. The actuators are retractable and orientable multilayer piezoelectric tabs which protrude perpendicularly from the model surface. They are mounted along the spanwise direction with constant spacing. The effectiveness of the control was tested in pre-critical and in post-critical regime by evaluating the effects of several control parameters of the tabs like frequency, amplitude, height, angular position and plate incidence with respect to the local flow. Measurements of the mean static pressure distribution around the cylinder were used to estimate the pressure drag coefficient. The maximum drag reduction achieved in the pre-critical regime was of the order of 30%, whereas in the post-critical regime was about 10%, 3% of which due to active forcing. Furthermore, pressure fluctuation measurements were performed and spectral analysis indicated an almost complete suppression of the vortex shedding in active forcing conditions.

Keywords: flow control; bluff body; cylinder; drag reduction; piezoelectric actuators; smart tabs

1. Introduction

The close relation between the aerodynamics of ground transportation vehicles and the flow control around bluff bodies has always motivated the fluid dynamics community, especially nowadays under the pressure of the well-known arguments related to pollutants emissions. A substantial contribution to solve the pollution problem may come from efficient flow control techniques focused on drag reduction through separation delay. Moreover, flow unsteadiness is originated by flow separation due to the shedding of large organized flow structures which influences the vehicle performance. Drag and vortex shedding are in fact strictly related as shown by Roshko (1955).

The basic idea underlying the flow separation suppression is related with enhancement of momentum in the near wall region of the boundary layer to overcome the effects of the adverse pressure gradient that tends to detach the flow. To this end, generation of streamwise vortex embedded into the boundary layer has been demonstrated to be very effective and vortex gen erator devices have been applied successfully in real applications as reported by Lin (2002) in an exhaustive review. A vortex generator configuration involves several geometrical parameters that

*Corresponding author, Professor, E-mail: gaetano.iuso@polito.it
[a] Ph.D., E-mail: matteo.orazi@polito.it
[b] Ph.D., E-mail: davide.lasagna@polito.it

http://www.techno-press.org/?journal=aas&subpage=7 ISSN: 2287-528X (Print), 2287-5271 (Online)

determine a very complex work of optimization. Counter-rotating arrays of streamwise longitudinal vortices generated by a spanwise row of vortex generators have shown beneficial effects as reported by Angele (2005), Godard and Stanislas (2006) among others. Sharma and Deshpande (2010) investigated on the effects of co-rotating and counter-rotating streamwise vortices in the wake of a 2D blunt trailing edged airfoil generated by prismatic appendages of trapezoidal shape positioned at regular spanwise intervals. The vortex shedding was suppressed thereby attenuating the drag and the unsteadiness. Griffin and Hall (1991) focused their review on the vortex shedding resonance and its control in the wake of bluff bodies. A complete and recent review on control methods for flow over bluff bodies including successful techniques, such as 3D forcing and active feedback control, was done by Choi *et al.* (2008). These authors classified the techniques as boundary-layer control and direct-wake modification and also discussed the Reynolds number dependence and the highest possible drag reduction and the control efficiency. Park *et al.* (2006) mounted a spanwise row of tabs perpendicular to the flow over a bluff body with blunt trailing edge. With these passive devices the authors obtained a 30% base pressure increase and the suppression of vortex shedding. The mismatch in the vortex shedding process introduced by the tabs originated an attenuation of the vortical strength in the wake. Pujals *et al.* (2010) achieved flow separation suppression on the rear-end of a 3D Ahmed body by means of large scale coherent streaks due to streamwise vortices generated by cylindrical roughness. Drag reduction up to 10% was observed when the roughness array was positioned upstream the separation line at 4-5 the spanwise spacing of the cylinders.

A promising active flow control technique easily implemented in closed-loop is that related to the synthetic jets due to the possibility of originating a broad range of time and spatial scales for flow manipulation. A vast review is presented by Glezer and Amitay (2002) which discusses isolated synthetic jets and their applications to several typology of flows. Béra *et al.* (2000) controlled the flow around a circular cylinder in post-critical conditions using synthetic jets actuators in open-loop configuration. The forcing resulted in lift and slightly increased drag. Shtendel and Seifert (2012) adopted fluidic actuators based on suction and oscillatory blowing to control the flow separation around a circular cylinder at transitional Reynolds numbers. In optimal operation conditions a drag reduction up to 50% and a complete suppression of the vortex shedding were observed. Muddada *et al.* (2010) also used synthetic jets actuators with closed-loop control to drive the vortex shedding from a 2D circular cylinder at sub-critical Reynolds numbers. This flow control strategy was able to suppress completely the vortex shedding from the cylinder.

Thomas *et al.* (2008) present an active flow control technique based on single dielectric barrier discharge plasma (DBD) to delay flow separation and to suppress vortex shedding from a circular cylinder. The authors used steady and unsteady actuation and showed a complete inhibition of the shedding phenomena. The most effective dimensionless actuation frequency in the unsteady forcing condition was equal to the unit. A plasma based flow control technique was also investigated by Ng *et al.* (2013) which used a streamwise-oriented DBD device on a circular cylinder. The actuator originated counter-rotating streamwise vortices capable of delaying flow separation in a limited region downstream the location of the electrode. These effects resulted in an enhancement of both lift and drag on the cylinder. Jukes and Choi (2009) maximized the lift with minimum increase of the drag of a circular cylinder making use of dielectric-barrier-discharge plasma actuators in pre-critical flow condition. An increase in lift of 300% was generated with an increasing of drag lower than 25% positioning the actuator 7° upstream of the separation point. All active flow control techniques require a certain amount of energy and therefore it is of crucial importance to evaluate an energy budget for most of real applications. In this regard, the

piezoelectric actuators are promising devices. In fact, they exhibit lower energy consumption with respect to other type of actuators and offer the possibility to recover energy during the passive phase of the element deformation. Most of the investigations on piezoelectric actuators as flow control devices are concentrated on the aeronautical field. Haller *et al.* (2009) designed, fabricated and applied a piezoelectric microactuator for dampening disturbances in the boundary layer of an airfoil reducing the amplitude of the Tollmien-Schlichting waves by 42%. Naim *et al.* (2002) used passive and active techniques to control the flow around a cylinder at transitional Reynolds numbers. In particular, the authors, using piezo-fluidic actuators, showed the capability of delaying flow separation evidencing two possible mechanisms of suppression.

In this paper, an experimental investigation on a cylinder, with the aim of controlling the flow separation using an open-loop technique based on piezoelectric actuators, is presented. The actuators (smart-tabs) mount rectangular piezoelectric tabs that act as vortex generators and can operate in passive or active conditions. In the latter case the control parameters, namely the frequency of oscillation and the amplitude can be independently changed. Eleven rectangular tabs are mounted in the spanwise direction and are equally spaced. Their orientation γ with respect to the local flow direction can be varied from parallel to perpendicular. Furthermore, the wall normal extension of the tabs can be varied from flush up to several local boundary layer thicknesses. The orientation of single tabs can be set independently allowing parallel or alternate configurations for an equal orientation angle γ. The circumferential location of the actuation θ_{tabs} can also be changed by rotating the cylinder around its axis. Results concerning the effects of some of the geometric tabs configuration, their location, and the effect of the frequency and amplitude of oscillation are presented. Most of the investigations are performed in post-critical regime where it is difficult to achieve separation delay with respect to the natural flow.

The main motivation of this paper is the development of an effective flow control technique with the aim to delay flow separation on a cylinder in post-critical regime. In fact, most of the investigations in literature are related to sub-critical Reynolds numbers where the drag reduction achieved is essentially due to the promotion of the boundary layer transition.

2. Experimental setup

The experimental investigation was arranged in a blowing wind tunnel with closed test section. The contraction area ratio was equal to 9.5 allowing a maximum freestream velocity of V_∞= 12 m/s and a turbulence level of about 0.4%. The test section was characterized by height, width and length equal to 0.9 m, 1.2 m and 1 m, respectively. The model was a circular cylinder with a diameter of 200 mm spanning from wall to wall in vertical direction. A turbulence generating grid was mounted at the entry of the test section in order to promote transition and achieve the post-critical regime. After the installation of the grid the turbulence level of the incoming flow was 6.5%. The model was positioned at 40 mesh lengths from the grid as suggested by Laws and Livesey (1978).

A 22 mm wide and 0.6 mm deep flattening was realized along a generatrix of the cylinder to host a row of 11 actuators spaced by 40 mm. The actuators consisted in rectangular piezoelectric elements with dimensions 45 x 11 x 0.6 mm mounted in cylindrical supports that allow the variation of their angle of attack γ. These supports are flush-mounted with respect to the model wall and contain a small piston which permits the height adjustment. The smart-tabs are characterized by two types of control parameters: geometric and dynamic. The latter are the

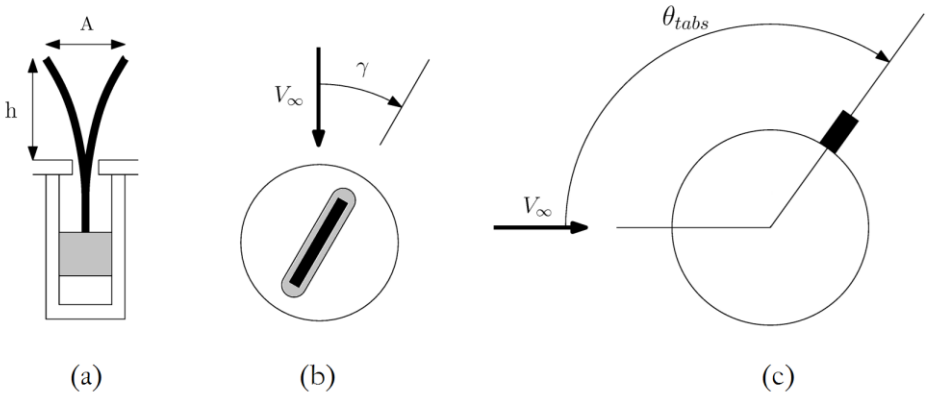

Fig. 1 Control parameters: (a) Smart-tab side view, (b) Smart-tab top view and (c) cylinder side view

oscillation frequency f , the oscillation amplitude A, and the input signal waveform. The geometric parameters include the height h, the angle of attack γ and the angular position on the model θ_{tabs}. The quantity θ is used to indicate the generic angular coordinate on the cylinder with respect to the undisturbed flow. Fig. 1 shows a sketch that illustrates the above mentioned parameters.

The key features of the smart-tabs are their low energy absorption and the energy recovery which makes them promising for real applications. Furthermore, considering their control characteristics and their frequency response, the piezoelectric tabs are suitable for closed-loop control strategies. An investigation related to the power absorption of the actuators was performed using a commercial wattmeter with a full scale of 3500 W and an accuracy of 0.1 W.

In the present study, measurements of static and fluctuating wall pressure were performed using static pressure taps and electret microphones respectively. Fig. 2 shows the actuators and the static and fluctuating pressure taps. A central section of the cylinder was equipped with 28 pressure taps spaced 10° on the 200° circular sector on the side of the actuators and 20° on the remaining part. The aerodynamic coefficients of the cylinder were evaluated by integration of the pressure distributions. The cylinder was also equipped with three spanwise rows of 12 pressure taps spaced 20 mm positioned at −10°, +10° +30° with respect to the actuators.

A second section of the cylinder was equipped with 15 pinhole mounted standard 9.8 mm diameter electret microphones with a flat response in the range 20 Hz - 15 kHz. To consider the attenuation in the microphones response below 20 Hz and to ensure an identical gain of all transducers, the microphones were calibrated using an high quality Brüel & Kjæ r microphone with flat response from 2 Hz up to 100 kHz. This calibration consists in the design of a Wiener filter using the signals originated by the 15 microphones and the Brüel & Kjæ r under a known white noise. The calibration procedure was performed in a tube with a length of 750 mm and a diameter equal to 150 mm.

At one end a loudspeaker was mounted, while on the opposite side a Plexiglas plate hosting all the transducers (B&K and the 15 microphones), was positioned. The B&K transducer was flush-mounted while the electret microphones were pinhole-mounted as on the cylinder to consider also the attenuation due to the pinhole mount. This kind of mounting was chosen to enhance the spatial resolution of the transducers and to avoid geometrical modifications of the curved cylinder wall introduced by a flush mount.

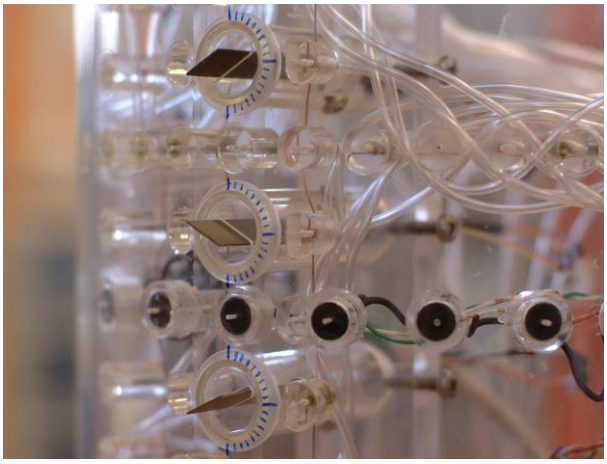

Fig. 2 Smart-tabs on cylinder ($\gamma = \pm 30°$)

The mean static pressure were acquired through a Scanivalve ZOC33 miniature pressure scanner with 64 pressure inputs taps with a full scale long term accuracy of ±0.08%. This module was placed inside the cylinder and thermally isolated using foam rubber. Preliminary investigations related to accuracy and convergence of the results required an acquisition time of 10 minutes at a sampling frequency of 40 Hz. For what concerns the pressure fluctuations, four National Instruments NI 9215 (4-Channel, 100 kS/s/ch, 16-bit) modules were employed. The data sets were of 2^{18} samples collected at a frequency of 10 kHz. Simultaneous sampling was adopted for the 15 microphones. Several boundary layer velocity profiles measurements were performed around the cylinder for the case of natural flow using a miniature total pressure probe having external diameter equal to 0.25 mm.

3. Results

Pressure distributions around the cylinder, pressure drag coefficients and spectral analysis of the pressure fluctuations are presented considering the effects of the flow control parameters previously introduced. Drag variation color maps are also shown considering the drag of the natural flow as reference. In the maps the grey dots indicate the measurements points, while the rest of the maps are obtained by linear interpolation. Some results concerning the pre-critical flow conditions are first presented while most of the analysis is concentrated on the post-critical condition, being of major interest and currently the most challenging objective concerning the flow control around a cylinder. It should be noted that the results related to pressure drag variations do not take into account the profile drag of the smart-tabs.

3.1 Pre-critical regime

Fig. 3 reports the pressure coefficient distributions around the cylinder at Re = 52000 for the case of tabs aligned with the local flow direction ($\gamma = 0°$) and without the turbulence generating grid. In particular, Fig. 3(a) refers to the natural flow while Figs. 3(b)-(c) are related to the cases of

tabs set at h = 5 mm, in static and forced conditions respectively. The pressure distribution related to the potential flow is also displayed in the same figure. For the case 3(c) the frequency of oscillation was set to f = 80 Hz corresponding to a reduced frequency of $F^+ = f\,h/V_\infty = 0.106$. The tabs were located at an angular position on the cylinder corresponding to $\theta_{tabs} = 75°$. The thickness δ of the boundary layer, measured in natural flow condition and in correspondence of the tabs location, was equal to 2.5 mm.

As can be observed comparing the case of natural flow (Fig. 3(a)) and that of static forcing (Fig. 3(b)) only small differences in the pressure distributions are present. Relatively higher suction peaks and a slight higher pressure recovery are present on the front and the back of the cylinder respectively. For both cases there is laminar separation, however the effect of the tabs gives rise to a drag reduction of the order of 6%. Greater effects are originated by the oscillation of the tabs (Fig. 3(c)) especially on the upper part of the cylinder. In fact, the pressure distribution is asymmetric due to the positioning of the tabs only on one side of the cylinder and a turbulent separation appears on the same side. On the lower part the pressure distribution is also affected

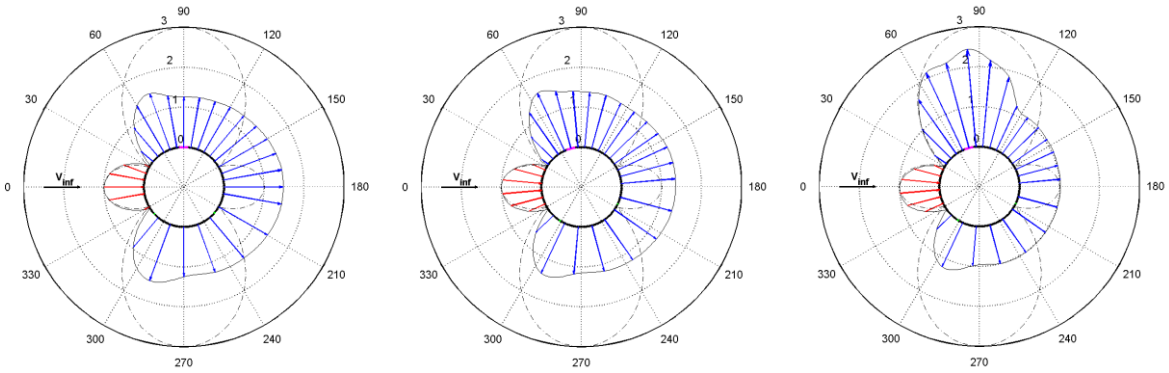

(a) h = 0 mm, f = 0 Hz (b) h = 5 mm, f = 0 Hz (c) h = 5 mm, f = 80 Hz

Fig. 3 C_p distrubutions, Re = 52000, $\gamma = 0°$: (a) Natural C_{dp} = 1.341, (b) Static C_{dp} = 1.262 and (c) Forced C_{dp} = 0.943

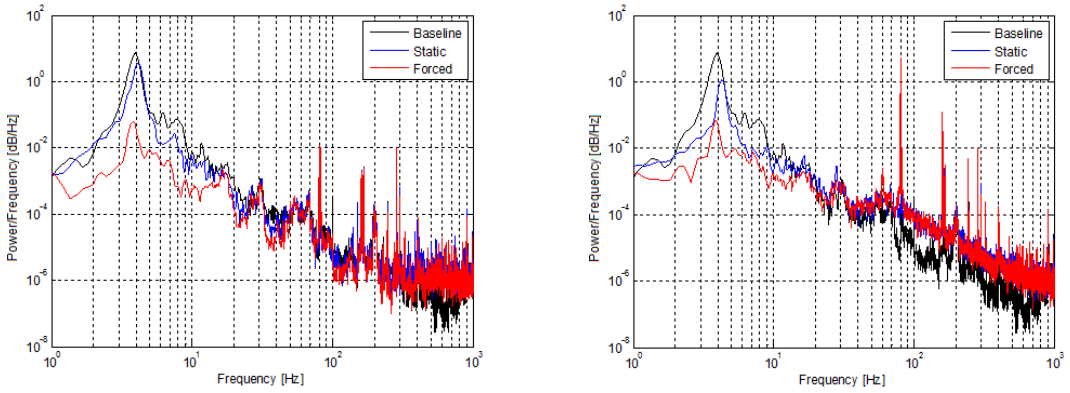

(a) $\gamma = 0°$ (b) $\gamma = 90°$

Fig. 4 PSD for Re = 52000, $\theta_{mic} = 90°, \theta_{tabs} = 75°$, h = 5 mm, f = 80 Hz

and, although the flow separation remains laminar on this side, the level of pressure is higher with respect to the previous cases. In Fig. 3(c) the pressure drag reduction is around 30%. The major effect of the dynamic forcing seems to be related to the promotion of the transition of the laminar boundary layer under the effects of the oscillating tabs. It is also evident that the disturbance introduced by the static tabs into the wall flow is not sufficient to cause a full transition (Fig. 3(b)).

Power spectral density of the fluctuating pressure signals are shown in Fig. 4. The results refer to the microphone positioned at $\theta = 90°$, in the case of natural and forced flows with static and active tabs, set at $\gamma = 0°$ (a) and $\gamma = 90°$ (b). The forcing frequency is f = 80 Hz for the forced cases. The tabs location and the protrusion are $\theta_{tabs} = 75°$ and h = 5 mm respectively.

Pressure fluctuation for the uncontrolled flow exhibit a peak of energy centered at f = 3.98 Hz which corresponds to a Strouhal number equal to 0.199, as expected. It is well evident that in the case of static aligned plates ($\gamma = 0°$, Fig. 4(a) the peak of energy is not greatly modified with respect to the natural flow, suggesting that the vortex shedding is not significantly influenced. On the other hand the dynamic forcing considerably affects the spectra in the low frequency range, up to f = 20 Hz, attenuating the amplitude roughly by two orders of magnitude with respect to the natural case. The high frequency range is not strongly affected by the forcing. The case of normal tabs with respect to the flow ($\gamma = 90°$, Fig. 4(b) highlights a similar behavior. The static forcing now is more effective in attenuating the vortex shedding with respect to the case of aligned tabs. The dynamic forcing is capable to further weaken the shedding lowering the energy distribution around the vortex shedding frequency. Comparing the results of case a and case b, it can be said that the vortex shedding is attenuated more in the case of static forcing by flow normal tabs than by aligned tabs. In the case of dynamic forcing the attenuation of the amplitude at the shedding frequency is nearly the same but the energy attenuations in the range of frequency 1 Hz - 20 Hz is higher when the tabs are aligned. It is not easy to explain this result, but it can be argued that the behavior is related to the interaction between the three-dimensional vortical system generated by the tabs and the flow in the wall region of the cylinder. Park et al.(2006) explained their results related to passive tabs set normally to the flow by considering the spanwise mismatch in the vortex-shedding process that originated a considerable reduction of the vortical strength in the wake. The pressure distributions reported in Fig. 3 are linked with the results showed by the spectra of Fig. 4(a) as it was expected. The amount of drag reduction appears in relation with the reduction of the pressure fluctuations energy. This behavior is not surprising because of the strict relation between drag and turbulent fluctuations, as reported by Roshko(1955).

3.2 Post-critical regime

An example of pressure distribution for uncontrolled flow in post-critical regime (Re = 115000) is shown in Fig. 5.

As can be seen, the grid gives rise to a complete transition on both sides of the cylinder determining a symmetric pressure distribution. The flow separates on the rear part of the cylinder at an angle $\theta = 120°$ with respect to the free stream direction.

In the following, drag variations are presented in form of color maps. The pressure drag coefficient assumed for the natural flow is that corresponding to the tabs configuration h = 0 mm and f = 0 Hz and pertaining to each angular position of the tabs. This was done to take into account the effects on the pressure distribution due to the small flattening on the cylinder that varied according to the angular position of the actuators θ_{tabs} .

In Fig. 6 results are reported varying the location θ_{tabs} of the tabs around the cylinder and the

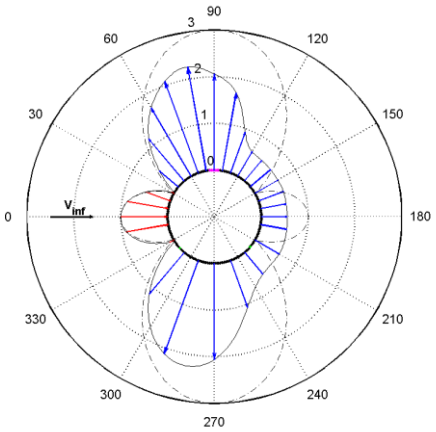

Fig. 5 Super-critical (Re = 115000) natural flow Cp distribution

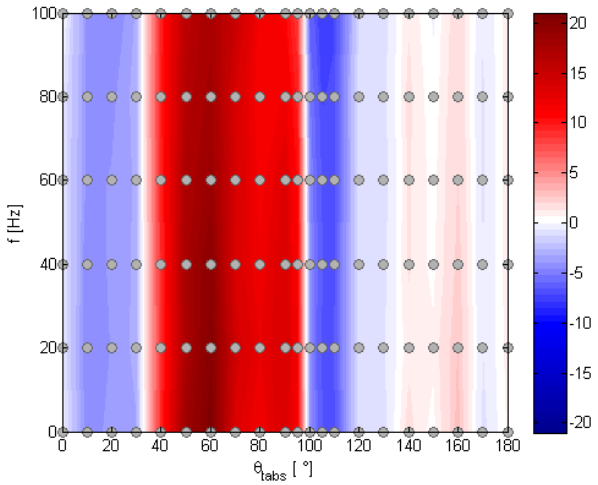

Fig. 6 Drag variations color map (h = 10 mm, $\gamma = \pm 30°$, A = A_{max})

oscillation frequency for a fixed value of the tabs height h = 10 mm and for the maximum oscillation amplitude of the tabs. The tabs are mounted in an alternate incidence configuration at $\gamma = \pm 30°$, as shown in Fig. 2. The case of static forcing is that corresponding to f = 0 Hz on the map. As can be observed, the drag variation strongly depends on θ_{tabs} . In the range $0° < \theta_{tabs} < 30°$ a drag reduction of the order of 4% is always present whichever is the forcing frequency.

This result is essentially due only to the contribution of static forcing. From $\theta_{tabs} = 35°$ to $\theta_{tabs} = 98°$ the effects of forcing change drastically, originating a drag increase due to the static forcing. Interestingly, as will be analyzed later in the paper, the effect of the active forcing gives an alleviating contribution also in this region. When the tabs are in the natural flow separation region, $98° < \theta_{tabs} < 120°$, they give rise to a drag alleviation of the order of 8%. This is the region where the tabs are the most effective as also reported in literature for different type of actuators. Positioning the tabs further downstream, for $120° < \theta_{tabs} < 180°$, does not generate any appreciable influence on the drag coefficient. For what concerns the effects of active forcing, it appears that

they are of small amount. Nevertheless it is evident the trend shown by the blue areas (drag reduction) that get wider and darker as the frequency increases.

Moreover, the drastic changes of sign of the drag variation in correspondence of specific values of the tabs location (θ_{tabs} = 35°; θ_{tabs} = 98°; θ_{tabs} = 120°) is interesting. This result is certainly related to the interaction between the tabs and the local flow around the cylinder according to the angular position θ_{tabs} . It is likely that the tabs positioned near the separation point with incidence set to $\gamma = \pm 30°$ behave as canonical vortex generators which originate counter-rotating streamwise vortices. However near the stagnation point another flow scenario could be present due to the tab height-wise direction of the incoming flow.

Based on the results of Fig. 6 in the following the tabs location was fixed at $\theta_{tabs} = 105°$ and the effects of the oscillation amplitude, the height and the incidence γ of the tabs were investigated. The thickness of the incoming boundary layer in this position on the cylinder ($\theta = 105°$) for the natural flow case was equal to $\delta = 5$ mm.

In Fig. 7 the frequency-amplitude drag variation color map is reported, where the array configuration ($\gamma = \pm 30°$) and the tabs height (h = 10 mm) were kept constant. The amplitude is displayed as percentage of the maximum value for each frequency tested. As for the previous case, the percentage variations indicated in Fig. 7 refer to the natural flow (h = 0 mm and f = 0 Hz). However, the color scale is centered (white color) on the drag reduction value related to the static condition. In this way, the map highlights the regions where the contribution to drag reduction is due to the active forcing.

From the map it is evident that the major contribution to drag reduction derives from the static forcing. Moreover, the map shows that significant dynamic contributions to the drag reduction are achieved for combinations of high values of forcing frequency and amplitude. In fact, the beneficial effects of the oscillation are located in the upper-right part of the map. From this point of view it would be desirable to have higher power actuators. In fact, given the trend shown in Fig. 7 and also in the previous map, it is likely that actuators able to oscillate at higher frequencies and/or amplitude could give a much higher drag reduction.

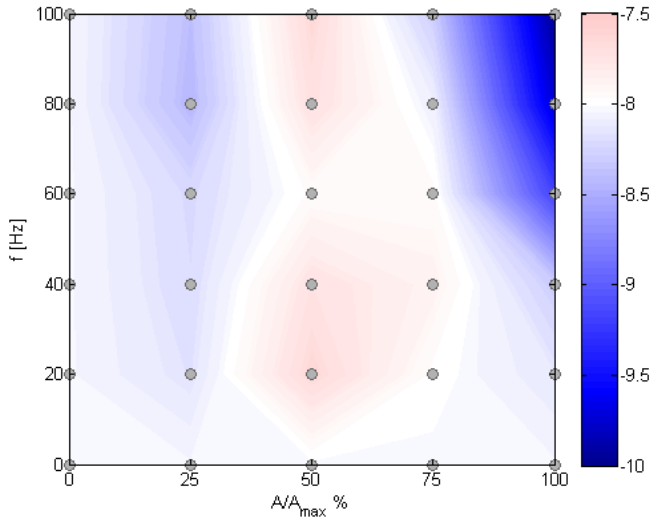

Fig. 7 Drag variations color map (θ_{tabs} = 105°, $\gamma = \pm 30°$, h = 10 mm)

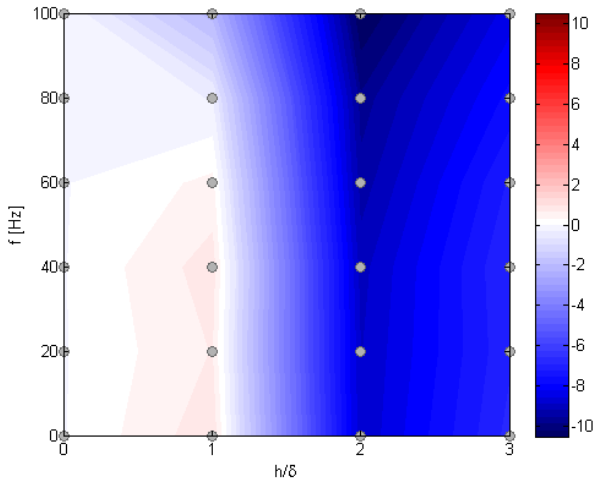

Fig. 8 Drag variation color map (θ_{tabs} = 105°, γ = ±30°, h = 10 mm, A = A_{max})

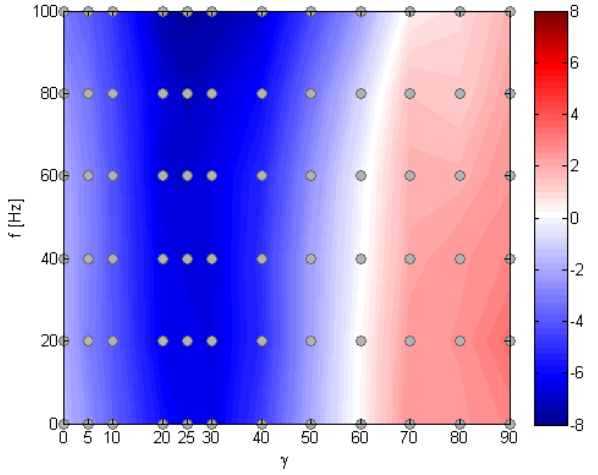

Fig. 9 Drag variation color map (θ_{tabs} = 105°, h = 10 mm, A = A_{max})

In Fig. 8 the map frequency - height is reported, where the oscillation amplitude is fixed to the maximum value.

No significant effects are observable for $h/\delta < 1$ unless very high frequencies are imposed. The highest drag reduction was achieved for $h > \delta$ and comes mainly from the static contribution. In particular, for $h/\delta = 2$ a drag reduction of about 8% was obtained in static condition while the frequency effect gives a further contribution up to 2% for f = 100 Hz. While the parameter h strongly influences the static effect of the tabs, it does not seem to play a key role for what concerns the dynamic contribution to drag reduction, which is about 2% for all the cases investigated.

The results related to the map frequency - incidence are presented in Fig. 9.

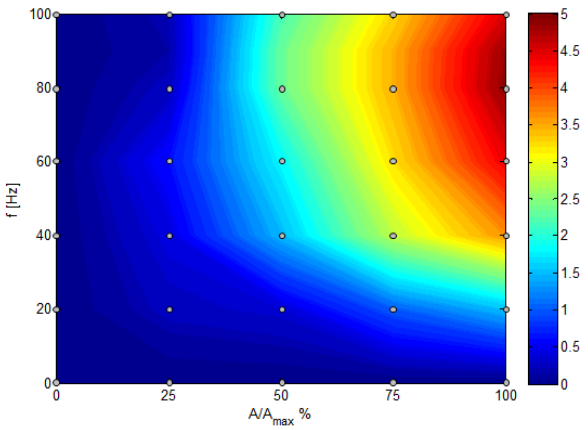

Fig. 10 Smart-tabs power absorption [W]

The tabs in static condition appear effective already for the case $\gamma = 0°$, although their effect is rather small. As γ increases the drag reduction also rises, reaching a peak of the order of 6.4% at about $\gamma = 30°$. For $\gamma > 60°$ the drag increases continuously as γ approaches 90°. The effects of the dynamic contribution are evidenced especially by the right oriented lines of iso-drag variation. In particular, for $60° < \gamma < 70°$, the iso-line $\Delta C_d/C_d = 0$ starts vertical from the static condition and then turns right as the frequency rises, restricting the drag increase region and enlarging the drag reduction one. It is likely that much higher values of frequency would have cancelled completely the red color from the map. This result suggests that a drag reduction could be achieved for every angle of attack of the tabs, if the forcing frequency is sufficiently high.

Fig. 10 reports the power consumption color map of the actuators in a frequency - amplitude map. The measurements reported, expressed in Watts, refer to the 11 actuators operated in parallel, for h = 10 mm.

It appears clear that the power absorption increases with the dynamic forcing parameters. The maximum absorption is around 5 W in the case of maximum amplitude and not for the maximum frequency but for f = 80 Hz. For increasing frequency up to f = 100 Hz, the power absorption evidences a reduction for all the tested amplitudes. This is because the tab is approaching the resonance frequency, which is equal to f_{res} = 160 Hz. A favorable energy budget is however not yet been achieved with the present results. For this purpose the wake analysis will be important to evaluate the drag of the global system cylinder plus actuators. The experimental setup for this investigation is in progress.

In order to better highlight the static and the dynamic forcing effects in the flow manipulation, in Figs. 11(a)-(b) the data extracted from the color maps showed in Figs. 6 and 9 have been reorganized. The drag variations inherent to the static and to the dynamic forcing (at f = 100 Hz) are displayed as a function of the tabs location θ_{tabs} and of the tabs incidence γ. The sum of the two contributions gives the total drag variation indicated in the maps.

As can be observed from Fig. 11(a) the two contributions can be in cooperation giving both drag reduction or drag increase but they can also be in opposition. The cases for which both effects contribute to drag reduction for the locations around $\theta_{tabs} = 20°$and around $\theta_{tabs} = 105°$ are noteworthy. A similar behavior appears in Fig. 11(b), where the incidence γ is reported in abscissa.

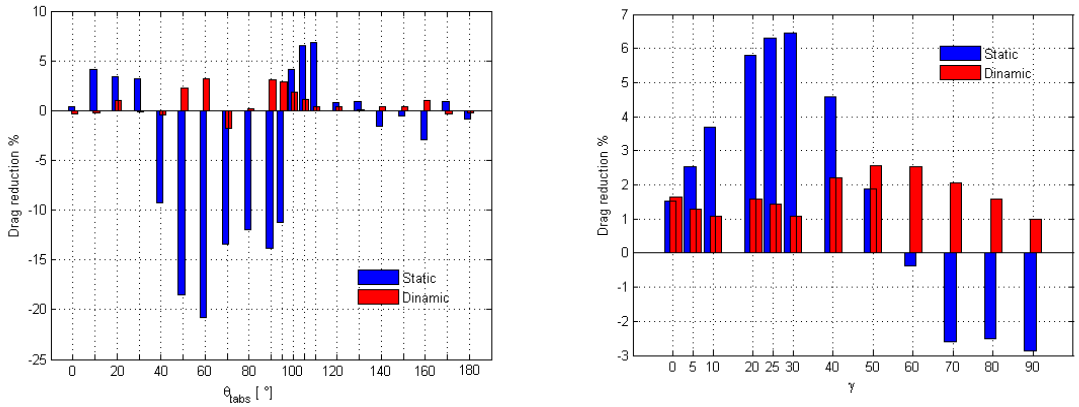

(a) $\gamma = \pm 30°$ (b) $\theta_{tabs} = +105°$

Fig. 11 Static and dynamic forcing contributions to drag reduction: (a) θ_{tabs} effect and (b) γ effect

A net distinction is evident between the range $0° < \gamma < 50°$ where both contributions to the drag variation concur to reduce drag and the range $60° < \gamma < 90°$ where instead the static effect gives rise to drag increases while the dynamic effect originates drag reduction. It is interesting to note that the dynamic effect is always drag alleviating whichever is the incidence of the tabs. Moreover, even though the dynamic contributions to drag reduction are not high, the indication emerging from the results is that a more powerful actuation would be needed.

Three typical incidences γ can be identified, characteristics of the flow generated by the tabs. Namely, $\gamma = 0°$ for which the effect of the oscillation originate a 3D vortical structure along the tip and the rear vertical side of the tabs. In the range of incidences around $\gamma = 40°$ the tabs work as small finite wings at incidence for which the main structure is the tip mean streamwise vortex structure. Finally, the range around the incidence $\gamma = 90°$ is typical for the generation of large region of separated flow behind a bluff body; also in this case a 3D vortical structure originates

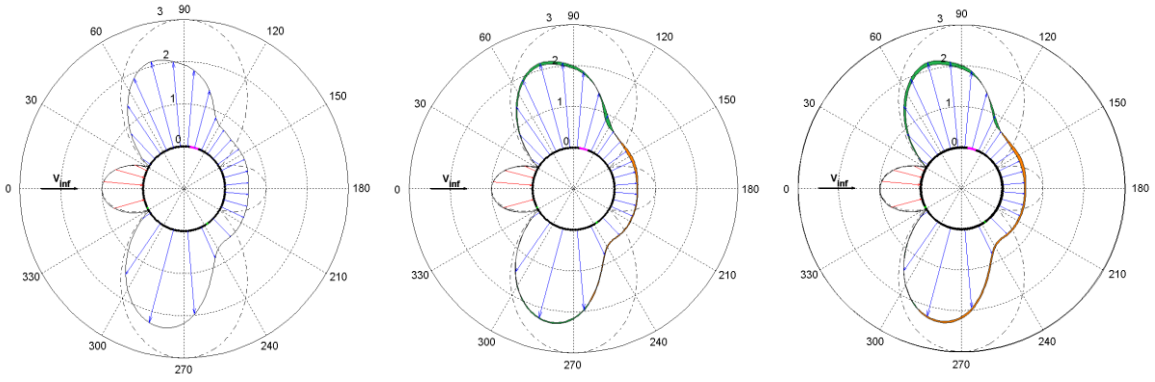

(a) h = 0 mm, f = 0 Hz (b) h = 10 mm, f = 0 Hz (c) h = 10 mm, f = 100 Hz

Fig. 12 C_p distributions, Re = 115000, $\gamma = \pm 30°$: (a) Natural $C_{dp} = 0.472$, (b) Static $C_{dp} = 0.441$ and (c) Forced $C_{dp} = 0.436$

from the three sides of the tabs. For all the incidences γ the effects of tabs oscillation could be linked with the intensification-weakening of the main 3D flow structures deriving from the tabs wake.

As an example of pressure distributions, in Fig. 12 the cases corresponding to θ_{tabs} = 105° for the natural flow (a), static forcing (b) and the dynamic forcing (c) are presented. The natural flow pressure coefficient contour is also reported in the cases (b) and (c), highlighting the differences with color areas. Green and orange indicate lower and higher pressure compared to the natural flow, respectively.

It can be observed that the three pressure distributions show a very similar behavior but some differences are evident in rear part and on the actuators side. In static forcing conditions (Fig. 12(b)), the flow separation is postponed and the flow detachment point moves from θ = 120° in the case of natural flow to θ = 125° evidencing, as a consequence, a better pressure recovery (orange). Furthermore, lower pressure (green) is observed between θ = 30° and θ = 95°, being this region mostly located on the front side of the cylinder, it contributes to drag reduction. The overall effect of the static forcing is a drag reduction of 6.54%. The dynamic forcing does not lead to a further delay of separation, however it contributes to a better pressure recovery that determines an extra drag reduction of 1.13%. Interestingly, while the static forcing affects only the pressure distribution on the actuators side, the dynamic forcing is able to slightly influence the pressure distribution also on the lower part of the cylinder.

For the same tabs position, θ_{tabs} = 105°, the power spectral density of the pressure fluctuations measured at θ = 105°, from a microphone located between two alternate tabs, is shown in Fig. 13 for the cases (a), (b) and (c) defined in Fig. 12.

The peak corresponding to the vortex shedding is less evident with respect to the laminar separation case as reported in Fig. 4. In fact, although a slightly higher level of energy is reached, the peak appears now smeared in the energy distribution of the spectra. The vortex shedding energy peak is identifiable for f = 8 Hz in the case of natural flow, to which corresponds for the Reynolds number equal to 115000 at a Strouhal number equal to 0.2, as expected. As can be seen the vortex shedding is suppressed in the cases of forced flow. Moreover, the spectra for the forced cases are affected not only at the forcing shedding frequency but also in the low frequency range up to f ≈ 60 Hz exhibiting lower level of energy respect to the natural flow.

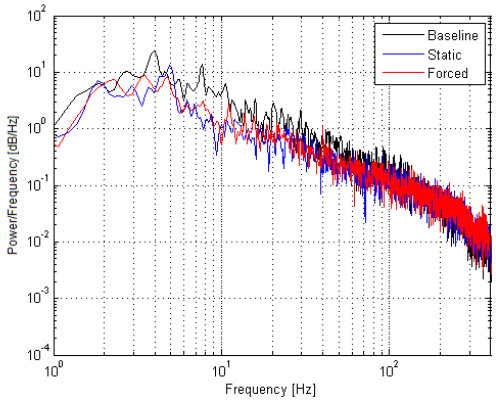

Fig. 13 PSD for Re = 115000, θ_{mic} = 105°, θ_{tabs} = 105°, h = 10 mm, γ = ±30°

4. Conclusions

An active flow control technique based on piezoelectric tabs was applied to a circular cylinder in pre-critical and post-critical regime.

The flow control technique was particularly effective in the pre-critical regime where the effects of the dynamic forcing was much more evident respect to the static one. For tabs aligned with the local flow ($\gamma = 0°$) and positioned at $\theta_{tabs} = -105°$, the tabs oscillation was responsible of a 30% drag reduction with respect to the natural flow, compared with the 6% of drag reduction obtained with the static forcing. The pressure distributions showed that the dynamic forcing in the pre-critical regime acts as transition promoter. Moreover, from the wall pressure fluctuations spectra an attenuation of the vortex shedding in condition of forced flow and especially in the case of dynamic forcing was also highlighted. The peak of energy at the vortex shedding frequency was weakened and around this frequency the energy content was also reduced.

In the post-critical regime the drag variation was greatly influenced by the location of the tabs around the cylinder, evidencing different ranges of θ_{tabs} for which alternate bands of drag reduction and drag increase were observed. The most beneficial effects were found when the actuators were located close to the flow separation point of the natural flow. The influence of the protrusion height was observed for values $h/\delta > 1$ and in particular for $h/\delta = 2$, for which the best result was achieved. The local incidence γ gave the major effects when in alternate configuration for values around $\gamma = \pm 25°$. The trends in drag variations showed that the larger the amplitude and the frequency of oscillation, the more effective is the control. An exploration of a larger parameter space in this direction should be performed. In the post-critical regime the highest drag reduction achieved was slightly above 10%. However, it has to be remarked that most of the drag reduction (7-8%) was due to the effects of the static forcing. In the post-critical regime the pressure fluctuations spectra also showed the attenuation of the vortex shedding. Furthermore, a lower energy in a wide range of frequencies around the peak related to the vortex shedding was observed, especially in dynamic forcing conditions.

The measurements of actuators power absorption evidenced a strong dependence on the oscillation frequency and amplitude. Interestingly, a reduction in power consumption was observed as the frequency approached the resonance frequency of the piezoelectric tabs.

It should be noted that the parasitic drag due to the smart-tabs was not taken into account in the results shown in the present paper. Wake investigations are currently being performed in order to evaluate the total drag of the cylinder including the smart-tabs drag.

References

Angele, K.P. and Muhammad-Klingmann, B. (2005), "The effect of streamwise vortices on the turbulence structure of a separating boundary layer", *Eur. J. Mech. - B/Fluids*, **24**, 539-554.

Béra, J.C., Michard, M., Sunyach, M. and Comte-Bellot, G, (2000), "Changing lift and drag by jet oscillation: experiments on a cylinder with turbulent separation", *Eur. J. Mech.- B/Fluids*, **19**(5), 575-595.

Choi, H., Jeon, W. P. and Kim, J. (2008), "Control of flow over a bluff body", *Ann. Rev. Fluid Mech.*, **40** 113-139.

Glezer, A. and Amitay, M.J. (2002), "Synthetic jets", *Ann. Rev. Fluid Mech.*, **34**, 503-529.

Godard, G. and Stanislas, M. (2006), "Control of a decelerating boundary layer. Part 1: Optimization of passive vortex generators", *Aero. Sci. Tech.*, **10**, 181 -191.

Griffin, O.M. and Hall, M.S. (1991), "Vortex shedding lock-on and flow control in bluff body wakes", *J.*

Fluid. Eng., **113** 526-537.
Haller, D., Hempel, J., Paetzold, A., Losse, N., Peltzer, I., Nitsche, W., King, R. et al. (2009), "A piezo-actuated closed loop MEMS system for active delay of transition", *TRANSDUCERS 2009. International Solid State Sensors Actuators and Microsystems Conference* doi:10.1109/SENSOR.2009
Jukes, T.N. and Choi, K.S. (2009), "Control of unsteady flow separation over a circular cylinder using dielectric-barrier-discharge surface plasma", *Phys. Fluids*, **21**, 094106.
Laws, E.M. and Livesey, J.L. (1978), "Flow through screens", *Ann.Rev. Fluid Mech.*, **10**, 247-266.
Lin, J.C. (2002), "Review of research on low-profile vortex generators to control boundary layer separation", *Porg. Aerosp. Sci.*, **38** (4-5), 389-420.
Muddada, S. and Patnaik, B.S.V. (2010), "An active flow control strategy for the suppression of vortex structures behind a circular cylinder", *Eur. J. Mech. - B/Fluids*, **29,** 93-104.
Naim, A., Seifert, A. and Wygnanski, I. (2002), "Active control of cylinder flow with and without a splitter plate using piezoelectric actuators", *1st Flow Control Conference* St. Luis, Missouri, AIAA paper 2002-3070.
Ng, J.H., Li, J., Cui, Y.D. and Lim, T.T. (2013), "Active flow control on a circular cylinder via streamwise-oriented dielectric barrier discharge plasma actuators", *51st AIAA Aerospace Sciences Meeting Including the new Horizons Forum and Aerospace Exposition*, Grapevine, Texas, AIAA 2013-0349.
Park, H., Lee, D., Jeon, W.P., Hahn, S., Kim, J.E., Kim ,J.U., Choi, J. and Choi, H. (2006), "Drag reduction in flow over two-dimensional bluff body with blunt trailing edge using a new passive device", *J. Fluid Mech.*, **563**, 389-414.
Pujals, G., Depardon, S. and Cossu, C. (2010), "Drag reduction of a 3D bluff body using coherent streamwise streaks", *Exp. Fluids*, **49**, 1085-1094.
Roshko, A. (1955), "On the wake and drag of bluff bodies", *J. Aeronaut. Sci.*, **22**,124-132.
Sharma, S.D. and Deshpande, P.J. (2010), "Innovative approach to generation of streamwise vortices in the wake of a blunt trailing edge", *37th National & 4th International Conference on Fluid Mechanics and Fluid Power*, December 16-18, 2010, IIT Madars, Chennai, India.
Shtendel, T. and Seifert, A. (2012), "Flow physics of bluff body drag reduction using active flow control", *EFMC9*, Rome, Italy.
Thomas, F.O., Kozlov, A. and Corke, T.C. (2008), "Plasma actuators for cylinder flow control and noise reduction", *AIAA J.*, **46**(8), 1921-1931.

EC